Developmental Maturation of the Precuneus as a Functional Core of the Default Mode Network

Rosa Li[1], Amanda V. Utevsky[1], Scott A. Huettel[1], Barbara R. Braams[2], Sabine Peters[3,4], Eveline A. Crone[3,4], and Anna C. K. van Duijvenvoorde[3,4]

Abstract

■ Efforts to map the functional architecture of the developing human brain have shown that connectivity between and within functional neural networks changes from childhood to adulthood. Although prior work has established that the adult precuneus distinctively modifies its connectivity during task versus rest states (Utevsky, Smith, & Huettel, 2014), it remains unknown how these connectivity patterns emerge over development. Here, we use fMRI data collected at two longitudinal time points from over 250 participants between the ages of 8 and 26 years engaging in two cognitive tasks and a resting-state scan. By applying independent component analysis to both task and rest data, we identified three canonical networks of interest—the rest-based default mode network and the task-based left and right frontoparietal networks (LFPN and RFPN, respectively)—which we explored for developmental changes using dual regression analyses. We found systematic state-dependent functional connectivity in the precuneus, such that engaging in a task (compared with rest) resulted in greater precuneus–LFPN and precuneus–RFPN connectivity, whereas being at rest (compared with task) resulted in greater precuneus–default mode network connectivity. These cross-sectional results replicated across both tasks and at both developmental time points. Finally, we used longitudinal mixed models to show that the degree to which precuneus distinguishes between task and rest states increases with age, due to age-related increasing segregation between precuneus and LFPN at rest. Our results highlight the distinct role of the precuneus in tracking processing state, in a manner that is both present throughout and strengthened across development. ■

INTRODUCTION

The human brain exhibits distinct patterns of functional connectivity between disparate brain regions, even when at rest. These patterns are so reliably evoked across studies and participants that they can be described as a set of canonical neural networks reflecting the intrinsic functional organization of the human brain (van den Heuvel & Hulshoff Pol, 2010; Smith et al., 2009). The default mode network (DMN), composed of the precuneus, posterior cingulate cortex, medial pFC, and bilateral TPJ, is the network most readily associated with rest states, as its activity increases during rest and decreases during task engagement (Raichle et al., 2001; Shulman et al., 1997). Other networks, however, also show patterns of intrinsic connectivity during rest, including lateralized frontoparietal networks (FPNs) that are more generally associated with task-positive, goal-directed attention (Vincent, Kahn, Snyder, Raichle, & Buckner, 2008; Corbetta & Shulman, 2002) and found to be anticorrelated with the DMN (Fox et al., 2005).

Across the regions of the DMN, the precuneus stands out for its distinctive role. Several studies have shown that, despite being a component of the DMN, precuneus activation increases during tasks such as memory retrieval (Lundstrom, Ingvar, & Petersson, 2005; Maddock, Garrett, & Buonocore, 2001; Fletcher et al., 1995), reward monitoring (Hayden, Nair, McCoy, & Platt, 2008), and emotion processing (Maddock, Garrett, & Buonocore, 2003; see Cavanna & Trimble, 2006 for a review). Notably, Utevsky, Smith, and Huettel (2014) found precuneus to be the only neural region that both increased connectivity with DMN at rest compared with at task and increased connectivity with the left FPN (LFPN) at task compared with at rest. Although greater precuneus–DMN connectivity during rest may be expected as a result of increased within-network connectivity, the finding of greater precuneus–LFPN connectivity during task is more counterintuitive, as precuneus is not part of the LFPN. These results suggest that precuneus serves as a functional core of the DMN by altering its network connectivity to LFPN and DMN according to whether the brain is in a task or a rest state.

Although precuneus (and adjacent posterior cingulate cortex) connectivity has been studied using data from adults (Utevsky et al., 2014; Fornito, Harrison, Zalesky, & Simons, 2012; Leech, Braga, & Sharp, 2012; Leech, Kamourieh, Beckmann, & Sharp, 2011; Honey et al., 2009), the role of the precuneus in mediating between task and rest states has not yet been investigated across development. Previous work using resting-state data has

[1]Duke University, [2]Vrije Universiteit Amsterdam, [3]Leiden University, [4]Leiden Institute for Brain and Cognition

Journal of Cognitive Neuroscience 31:10, pp. 1506–1519
doi:10.1162/jocn_a_01426

shown that within-network functional and structural connectivity increases with age for DMN and FPNs (Baum et al., 2017; Uddin, Supekar, Ryali, & Menon, 2011; Fair et al., 2007, 2008) and that the DMN and FPNs become increasingly segregated from each other with age (Sherman et al., 2014), consistent with the idea that within-network connections are strengthened and between-network connections are weakened across development (Fair et al., 2009). Therefore, we expected that the precuneus, as a node of the DMN, would show developmental changes in connectivity with DMN and FPN, reflecting change in the degree to which this functional region mediates between task and rest states.

Here, we used network-based connectivity analyses to probe the role of the precuneus in a large accelerated longitudinal sample. Over 250 participants between the ages of 8 and 26 years completed a resting-state scan and two cognitive task scans at two longitudinal time points approximately 2 years apart. We used data from the first longitudinal time point to identify rest- and task-based networks of interest, DMN, and LFPN and right FPN (RFPN). We then used dual regression analyses

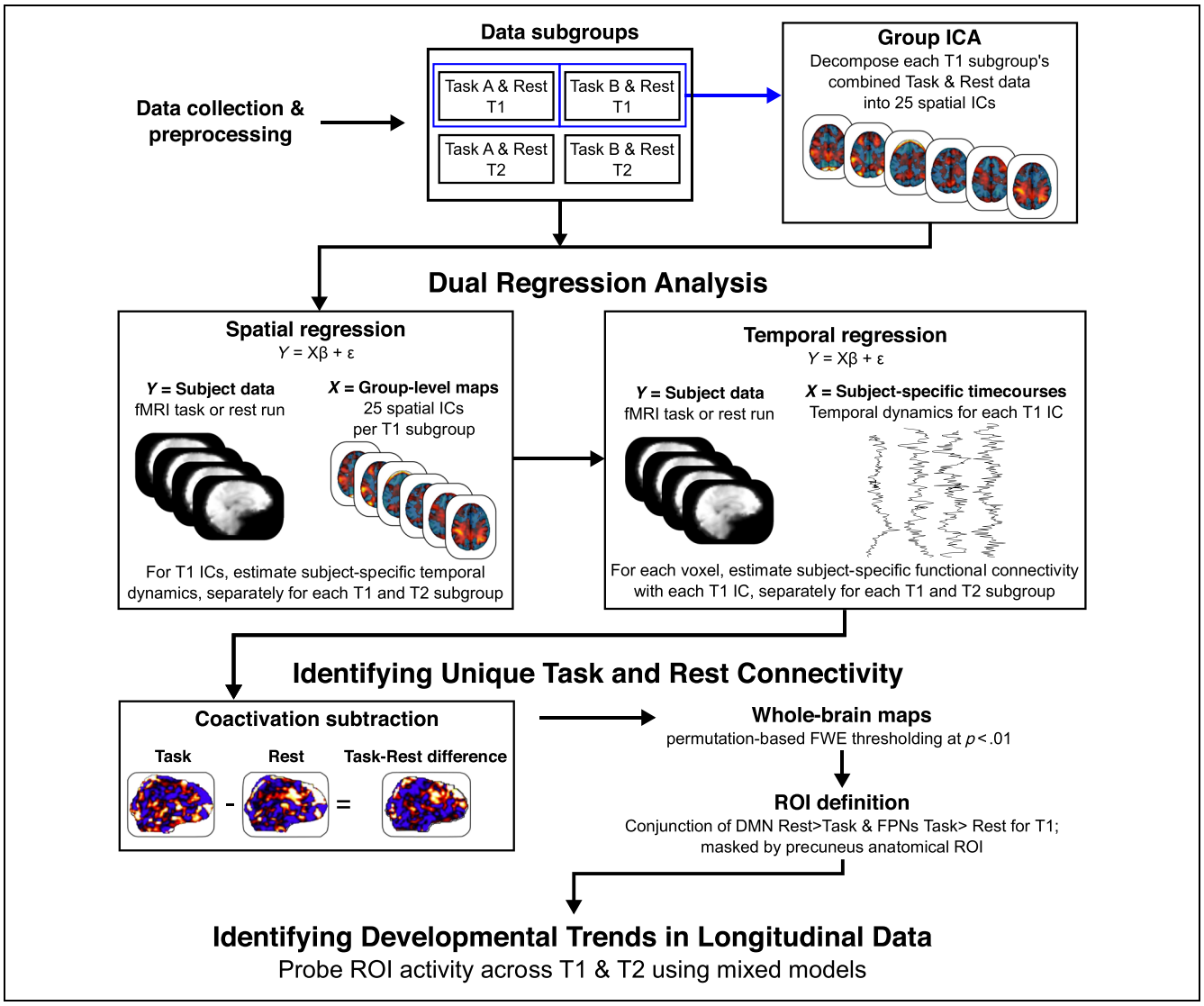

Figure 1. Schematic diagram of analytic approach (adapted from Utevsky et al., 2014). After data were collected and preprocessed, each task data set was paired with the corresponding rest data set for the same subgroup of participants. Data from two tasks across two developmental time points were used, resulting in four subgroups. Each T1 subgroup of combined task and rest data were entered into a group ICA, resulting in 25 spatial network maps for the T1 Task A + Rest data and another 25 spatial network maps for the T1 Task B + Rest data set. The network maps for each T1 task subgroup were then entered in separate dual regression analyses for each corresponding T1 and T2 task subgroup (e.g., T1 Task A + Rest network maps were used for a T1 Task A + Rest dual regression and a separate T2 Task A + Rest dual regression). This allowed us to quantify, for each participant, each voxel's connectivity with each network while controlling for the other 24 networks. Each participant's resting-state connectivity map was then subtracted from their task-state connectivity map, allowing us to examine within-participant connectivity differences for each of our networks of interest (DMN, LFPN, and RFPN). The resulting task–rest difference maps were submitted to permutation-based thresholding to examine statistically significant differences. Finally, precuneus ROI analyses were conducted by submitting task–rest connectivity differences at both time points to mixed models including age-related parameters.

(Nickerson, Smith, Öngür, & Beckmann, 2017; Smith et al., 2014; Leech et al., 2011, 2012; Filippini et al., 2009) to examine task versus rest connectivity with our networks of interest at both longitudinal time points and for both tasks (see Figure 1 for a schematic analysis diagram). This design allowed us to self-replicate connectivity results across two longitudinal time points and self-replicate developmental results across two different tasks. Our results extended previous findings in adults (Utevsky et al., 2014) to children and adolescents while also testing the hypothesis that the role of the precuneus as a functional core of the DMN strengthens across human development.

METHODS

Participants and Experimental Tasks

Data for the current study were drawn from the first two time points of a large longitudinal imaging study (BrainTime) that was conducted at Leiden University in the Netherlands. At the first longitudinal time point (T1), data were collected from 299 participants (mean age = 14.15 years, age range = 8.01–25.95 years; 156 female). Data at the second longitudinal time point (T2) were collected approximately 2 years later from 254 of the original participants (mean age = 16.07 years, age range = 9.92–26.62 years; 131 female). Although previous articles have published findings from the BrainTime study's resting-state data (van Duijvenvoorde, Westhoff, de Vos, Wierenga, & Crone, 2019; Peters, Peper, van Duijvenvoorde, Braams, & Crone, 2017; Peters, Jolles, van Duijvenvoorde, Crone, & Peper, 2015; van Duijvenvoorde, Achterberg, Braams, Peters, & Crone, 2015) and data from its two tasks separately (Schreuders et al., 2018; Braams & Crone, 2017a, 2017b; Peters & Crone, 2017; Peters, Van der Meulen, Zanolie, & Crone, 2017; Braams, Peper, Van Der Heide, Peters, & Crone, 2016; Peters, van Duijvenvoorde, Koolschijn, & Crone, 2016; Braams, van Duijvenvoorde, Peper, & Crone, 2015; Braams, Güroğlu, et al., 2014; Braams, Peters, Peper, Güroğlu, & Crone, 2014; Peters, Braams, Raijmakers, Koolschijn, & Crone, 2014; Peters, Koolschijn, Crone, van Duijvenvoorde, & Raijmakers, 2014), this is the first study integrating all of the functional task and rest data from BrainTime's first two longitudinal time points.

Written informed consent was obtained from adult participants, whereas parent consent and participant assent was obtained from minor participants under a protocol approved by the institutional review board of Leiden University Medical Centre. Participants were screened for MRI contraindications. All participants were right-handed, had no history of neurological or psychiatric disorders, and had their anatomical scans reviewed and cleared for incidental findings by a radiologist.

At both longitudinal time points, participants first completed a 5.1-min resting-state scan in which they were instructed to lie still with their eyes closed but remain awake. Then, participants completed two runs of a feedback learning task, in which they learned associations between stimuli through positive and negative feedback (Task A; Peters, Van der Meulen, et al., 2017; Peters et al., 2016; Peters, Braams, et al., 2014; Peters, Koolschijn, et al., 2014), followed by two runs of a self/other reward processing task, in which they guessed coin flip outcomes to win money for themselves or another person (Task B; Braams & Crone, 2017a, 2017b, Braams et al., 2015, 2016; Braams, Güroğlu, et al., 2014; Braams, Peters, et al., 2014). Finally, anatomical images were obtained.

Data were split into four subgroups based on longitudinal time point and task (e.g., the original T1 Task A + Rest subgroup consisted of all participants who, at T1, completed at least one run of Task A and the resting-state run). Within each subgroup, data were excluded based on data quality concerns (see Preprocessing section below) or for task performance indicating poor task engagement (performance less than three times the interquartile range in the feedback learning task; failing to make a response on >30% of trials in the reward processing task). These exclusion criteria left a final sample of 225 participants in the T1 Task A + Rest subgroup, 197 participants in the T1 Task B + Rest subgroup, 198 participants in the T2 Task A + Rest subgroup, and 187 participants in the T2 Task B + Rest subgroup. See Table 1 for demographics of each subgroup.

The final subgroups included 120 participants (67 female) who were in all four subgroups, 158 (84 female) participants who were in both Task A + Rest subgroups across longitudinal time points, 131 (75 female) participants who were in both Task B + Rest subgroups across longitudinal time points, 190 (103 female) participants who were in both T1 subgroups across tasks, and 177 (89 female) participants who were in both T2 subgroups across tasks.

Image Acquisition

Scanning was performed on a 3-T Phillips Achieva MRI system using a standard whole-head coil. Functional scans

Table 1. Participant Demographics for Each Subgroup

Group	*Final n (n Female)*	*Mean Age (years)*	*Age Range (years)*
T1 Task A + Rest	225 (116)	14.58	8.01–25.95
T1 Task B + Rest	197 (109)	14.82	8.01–25.95
T2 Task A + Rest	198 (102)	16.58	10.02–26.62
T2 Task B + Rest	187 (96)	16.75	10.02–26.62

were acquired using a T2*-weighted EPI sequence (repetition time [TR] = 2.2 sec, echo time [TE] = 30 msec, descending sequential acquisition of 38 axial slices, flip angle = 80°, field of view [FOV] = 220 × 114.7 × 220 mm^3, voxel size = 2.75 mm^3). The resting-state scan consisted of 142 volumes, each run of Task A consisted of 128–222 volumes, and each run of Task B consisted of 212 volumes. All functional runs included two initial dummy volumes to allow for signal equilibration. Experimental images were back-projected onto a screen that was viewed through a mirror.

Following functional scanning, a T1-weighted anatomical scan (TR = 9.76 msec, TE = 4.59 msec, flip angle = 8°, FOV = 224 × 168 × 177.3, 140 slices, voxel size = 1.17 × 1.17 × 1.2 mm, inversion time = 1050 msec) and a high-resolution EPI scan (TR = 2.2 sec, TE = 30 msec, 84 slices, flip angle = 80°, FOV = 220 × 168 × 220 mm^3, voxel size = 1.96 × 2 × 1.96 mm) were obtained to facilitate coregistration and normalization of functional data.

Preprocessing

Data were preprocessed using FSL Version 5.0.4's (Woolrich et al., 2009; Smith et al., 2004) FMRIB's Expert Analysis Tool, including motion correction by realignment to the middle volume of each time series (Jenkinson & Smith, 2001), slice-time correction, removal of nonbrain tissue (Smith, 2002), spatial smoothing using a Gaussian kernel of 6 mm FWHM, grand mean intensity normalization, and high-pass temporal filtering (Gaussian-weighted least squares straight line fitting with a 150-sec cutoff). Functional scans were first coregistered to the high-resolution EPI images, which were in turn registered to the T1 images, which were finally registered to the Montreal Neurological Institute avg152 T1-weighted template using FSL's Nonlinear Image Registration Tool.

For quality control, we examined five partially correlated measures of quality assurance for each run: (1) average signal-to-fluctuation-noise ratio (Friedman, Glover, & The FBIRN Consortium, 2006), (2) average volume-to-volume motion, (3) maximum absolute motion, (4) percentage of volumes with framewise displacement (*FD*) greater than 0.5 mm (Power, Barnes, Snyder, Schlaggar, & Petersen, 2012), and (5) percentage of outlier volumes with root-mean-square intensity difference relative to the reference volume (refRMS) greater than the 75th percentile plus the value of 150% of the interquartile range of refRMS for all volumes in the run (i.e., standard boxplot threshold for outlier detection). Within each participant's data for each task, we identified the "best" of the two runs as the run with the lowest percentage of refRMS outlier volumes and included only that run in subsequent analyses. Finally, within each task's best runs and within the resting-state data, we excluded the 95th percentile of worst runs for each data quality metric and/or ≥3 mm of motion and/or ≥10% poor quality volumes, whichever criteria was strictest (see Participants and Experimental Tasks section for final included sample sizes). This left us with one task and one rest run per participant in each analysis subgroup (i.e., each participant in the T1 Task A + Rest subgroup contributed one T1 Task A run and their T1 resting-state run to the analyses). Because each analysis subgroup drew from the same initial participant pool but faced slightly different percentile-based exclusion criteria, the exact makeup of each analysis subgroup included overlapping but nonidentical participants.

As even mild motion artifacts can distort connectivity analyses (Power et al., 2012; Satterthwaite et al., 2012), we implemented additional analyses to correct for motion issues. We regressed out variance tied to six motion parameters (rotations and translations along the three principal axes). Furthermore, for every run, we regressed out all volumes with *FD* greater than 0.5 mm and all refRMS outlier volumes. Though this is not identical to the scrubbing procedure of Power and colleagues (2012), it accomplishes the same goal of removing signal discontinuities and spurious effects of head motion that cannot be accounted for by conventional motion regression.

Independent Component Analysis

T1 data for each task + rest subgroup were run through separate probabilistic group independent component analysis (ICA; Beckmann & Smith, 2004). Each ICA had two inputs per subgroup participant: one resting-state scan and one task-based scan. Input data were first downsampled to 3 mm isotropic resolution using a 12-parameter affine transformation implemented in FSL's Linear Image Registration Tool (Jenkinson & Smith, 2001) to reduce data-processing demands. Through FSL's Multivariate Exploratory Linear Optimized Decomposition into Independent Components, data were voxel-wise demeaned and normalized, whitened, and projected into a 25-dimensional subspace (the number of selected components was based on Utevsky et al., 2014), resulting in 25 independent components (ICs) per subsample.

From each T1 task + rest subgroup's ICA output, we identified the ICs corresponding to our three networks of interest (DMN, RFPN, and LFPN) as those with the highest spatial correlation to the canonical network maps of Smith and colleagues (2009; Figure 2A). Spatial correlation values are reported in Table 2.

To check that the T1 task + rest ICs were robust to changes in participant groupings (see Methods: Participants and Experimental Tasks section), we ran three additional ICAs using the T1 data: one with the 120 participants who were in all four subgroups (provided useable data for all task and rest scans at both longitudinal time points), one with the 158 participants who were in both longitudinal time points' Task A + Rest subgroups, and one with the 131 participants who were in both longitudinal time points' Task B + Rest subgroups. The spatial

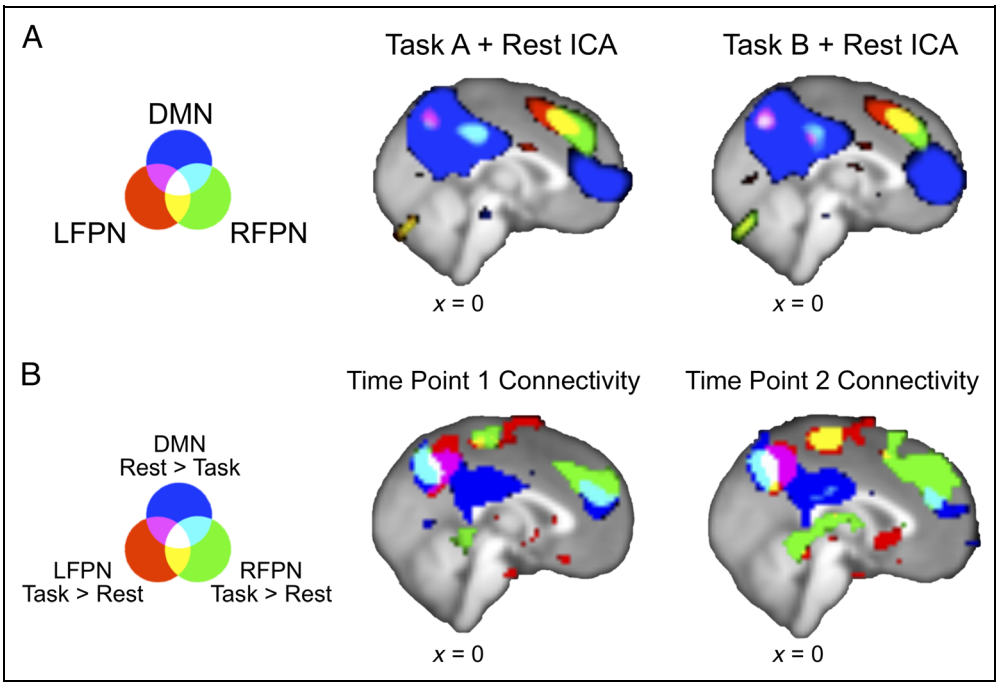

Figure 2. Task versus rest connectivity with DMN and LFPN and RFPN. (A) Canonical networks of interest from the T1 Task A + Rest and T1 Task B + Rest subgroups. Images thresholded at $2.3 < z < 4$. (B) Task versus rest connectivity for the three canonical networks of interest. Rest > task connectivity with DMN and task > rest connectivity with LFPN and RFPN show a conjunction over precuneus (white). FWE-corrected $p < .01$ with threshold-free cluster enhancement.

correlations between the DMN, LFPN, and RFPN from each of these new ICAs to the corresponding ICs used in our final analyses ranged from 0.945 to 0.997. This indicates that our identified ICs were largely consistent across the different subsets of participants.

Dual Regression Analysis

We examined changes in connectivity between task and rest states by submitting the network maps of each group's task and rest runs to dual regression analyses (as in Utevsky et al., 2014). Dual regression analysis quantifies voxelwise connectivity for each IC while controlling for the other ICs (Nickerson et al., 2017; Filippini et al., 2009). Each dual regression analysis comprised two stages (Figure 1). First, each IC map was regressed onto each run's functional data set, resulting in run-specific time courses for each IC. Second, those resulting time courses were then regressed onto each run's functional data to estimate each voxel's connectivity with each IC while controlling for the other 24 ICs.

Each task + rest group at T1 used its own ICs for its own separate dual regression analysis. So that the ICs entering the dual regression were consistent across longitudinal time points, T1 ICs were used for their corresponding T2 subgroups' dual regression. In other words, T1's Task A + Rest ICs were used for the dual regression analysis of T1 Task A + Rest and the dual regression analysis for T2 Task A + Rest, whereas T1's Task B + Rest ICs were used for the dual regression of T1 Task B + Rest and the dual regression analysis for T2 Task B + Rest.

Task–Rest General Linear Model

To investigate differences in task and rest connectivity within each participant, each participant's resting-state connectivity map was subtracted from their task–state connectivity map separately for each task (Task A > Rest; Task B > Rest), for each of the three networks of interest (DMN, LFPN, and RFPN) and at each longitudinal time point (T1 and T2). The resulting difference maps indicating task-minus-rest changes in connectivity with each network were entered into separate group-level general linear models for each task + rest subgroup, network, and longitudinal time point. To further control for spurious

Table 2. Spatial Correlations between ICA Outputs and Canonical Maps from Smith et al. (2009)

Canonical Network	*T1 Task A + Rest & Smith et al., 2009*	*T1 Task B + Rest & Smith et al., 2009*	*T1 Task A + Rest & T1 Task B + Rest*
DMN	.73	.80	.95
LFPN	.71	.74	.97
RFPN	.66	.63	.96

motion-related results that could arise from participants moving more during task than rest—above and beyond motion controls implemented during preprocessing—each model contained additional subject-level nuisance regressors representing individual differences in motion between task and rest: (1) difference in average signal-to-fluctuation-noise ratio, (2) difference in average volume-to-volume motion, (3) difference in percentage of volumes with *FD* greater than 0.5 mm, and (4) difference in percentage of refRMS outlier volumes. Finally, we included (5) an additional nuisance regressor to account for sex (Smith et al., 2014; Filippi et al., 2013). All nuisance regressors were demeaned.

We generated bidirectional contrasts comparing task and rest states in each of the three networks of interest for each task + rest subgroup at each longitudinal time point. Statistical significance was determined using Monte Carlo permutation-based statistical thresholding with 10,000 permutations, family-wise error (FWE)-corrected for multiple comparisons across the whole brain (Winkler, Ridgway, Webster, Smith, & Nichols, 2014). Activation clusters were estimated using threshold-free cluster enhancement (Smith & Nichols, 2009).

We conducted conjunction analyses across both tasks, separately for each longitudinal time point (i.e., conjunction of T1 Task A > rest with T1 Task B > rest; conjunction of T2 Task A > rest with T2 Task B > rest) for each network of interest using the minimum statistic (Nichols, Brett, Andersson, Wager, & Poline, 2005). This allowed us to examine neural connectivity during task states in general, rather than connectivity specific to Task A or Task B. These conjunction analyses resulted in a task > rest and a rest > task connectivity map for each network of interest (DMN, LFPN, and RFPN) and at each longitudinal time point.

ROI Identification

To restrict subsequent age-related analyses to our a priori ROI, we identified a precuneus ROI by masking the T1 conjunction of task > rest connectivity with LFPN, task > rest connectivity with RFPN, and rest > task connectivity with DMN (see Figure 2B) with the Harvard–Oxford atlas's anatomical precuneus ROI thresholded at 70% (Desikan et al., 2006). Participants' task and rest connectivity parameters were then extracted from this precuneus ROI for each longitudinal time point and network.

Experimental Design and Statistical Analysis

Age-related differences in connectivity parameters were further probed across data from both longitudinal time points using a mixed-model approach in R with the package *nlme* (Pinheiro, Bates, DebRoy, Sarkar, & R Core Team, 2019). Mixed models (also known as hierarchical linear models, multilevel models, or random-effects models) as applied to longitudinal data sets allow longitudinal time points to be nested within participants by modeling participant identity as a random effect. ROI mixed models were run on connectivity parameters combined across T1 and T2, separately for each task (e.g., T1 & T2 Task A + Rest data in one set of analyses; T1 & T2 Task B + Rest data in a separate set of analyses). This allowed us to self-replicate any developmental changes in task-versus-rest connectivity across two different tasks.

To test for significant developmental differences, we first fit a null, intercept-only model including a fixed and random intercept. We then compared the intercept-only model to three different age-related models: one with a mean-centered linear continuous age term to test for monotonic age-related changes; one with mean-centered linear and quadratic age terms to test for additional quadratic age-related changes (e.g., developmental peaks or troughs); and one with mean-centered linear, quadratic, and cubic age terms to test for additional cubic age-related changes (e.g., developmental changes that emerge and then stabilize; Madhyastha et al., 2018). Likelihood ratio tests between the intercept-only, linear, quadratic, and cubic models were used to determine whether the age-related models with significant age parameters significantly improved model fit over the intercept-only model or the next simplest model with a significant age parameter.

To rule out overall task performance or engagement as a confound for any significant age-related findings, we ran additional models adding a metric of task engagement as an additional regressor to any model with significant age-related findings that may have been driven by neural activity during task. The metric for Task A was participants' learning rates, as measured by the percentage of trials in which feedback was successfully used on the subsequent trial (Peters et al., 2016; Peters, Braams, et al., 2014). The metric for Task B was participants' self-reported liking of winning money for self, reported at the end of the scanning session (Braams et al., 2015; Braams, Güroğlu, et al., 2014; Braams, Peters, et al., 2014). Task B self-report metrics were not collected from 87 participants at T1 and 6 participants at T2. Consequently, task engagement control analyses for Task B were run with fewer participants (n = 248) and data points (n = 353) than the age-only models.

Table 3. Number of Participants and Data Points in Mixed-model Analyses

T1 & T2 Task + Rest Subgroup	*Participants n*	*Data Points n*
Task A + Rest: All participants	265	423
Task B + Rest: All participants	253	384
Task A + Rest: Task engagement analyses	265	423
Task B + Rest: Task engagement analyses	248	353

To rule out motion issues as a confound for any significant age-related findings, we ran additional models adding the percentage of volumes with *FD* > 0.5 mm for the task runs and the rest run as an additional regressor to any model with significant age-related findings.

RESULTS

Precuneus Connectivity Distinguishes Task and Rest States across Development

The whole-brain conjunction analyses across both tasks at each longitudinal time point show that precuneus is both significantly more connected with both LFPN and RFPN at task than at rest and significantly more connected with DMN at rest than during task (Figure 2B; Table 4). Thus, in our cross-sectional samples at both T1 and T2, we replicate Utevsky and colleagues' (2014) finding that precuneus connectivity distinguishes between tasks and rest states in adults via varying connectivity with DMN (rest > task) and LFPN (task > rest). Notably, we also extend this finding to connectivity with RFPN (task > rest) and to cross-sectional neural data from participants between the ages of 8 and 26 years.

The whole brain conjunction also indicated that lateral occipital cortex and pre/postcentral gyrus exhibited a similar connectivity profile to precuneus, though we note that the precuneus was the largest conjunction cluster at both longitudinal time points (Table 4). As we a priori hypothesized that precuneus would exhibit state-dependent connectivity changes (Utevsky et al., 2014), subsequent ROI analyses to probe developmental connectivity changes were conducted within our conjunction result, masked by a precuneus anatomical ROI (see Methods: ROI Identification section).

Task/Rest Connectivity Differences between Precuneus and LFPN Increase with Age

We applied mixed models to the longitudinal precuneus connectivity parameters extracted from our precuneus ROI. This allowed us to test for age-related changes in task–rest connectivity between the precuneus and each of the three networks of interest, while accounting for the repeated measures in our longitudinal data. Separate mixed models were applied to Task A + Rest data and to Task B + Rest data, which allowed us to use two different tasks to (1) self-replicate any developmental findings across tasks and (2) show that such findings are generalizable to task state rather than specific to a particular task.

We found a significant linear effect of age in task > rest precuneus connectivity with LFPN in both of the tasks

Table 4. Regions Exhibiting Task- and Rest-dependent Connectivity Changes with DMN and FPNs

Longitudinal Time Point	*Probabilistic Anatomical Label*	*x*	*y*	*z*	*p*	*Cluster Extent*
T1	Precuneus cortex (86%)	3	−63	33	< .001	152
	Inferior lateral occipital cortex (61%), occipital fusiform gyrus (9%)	−45	−75	−9	< .001	108
	Postcentral gyrus (51%), precentral gyrus (30%)	−60	−6	24	< .001	101
	Insular cortex (74%), frontal orbital cortex (8%)	−36	15	−12	.002	12
T2	Precuneus cortex (26%), cuneal cortex (18%), supracalcarine cortex (17%), intracalcarine cortex (9%)	12	−66	21	< .001	179
	Inferior lateral occipital cortex (50%), superior lateral occipital cortex (11%)	−39	−81	6	< .001	75
	Superior lateral occipital cortex (67%), precuneus (1%)	30	−69	51	< .001	71
	Precentral gyrus (23%), postcentral gyrus (19%), central opercular cortex (4%)	−57	−6	18	.003	63
	Frontal pole (87%)	−24	60	0	< .001	35
	Inferior lateral occipital cortex (39%), occipital fusiform gyrus (19%)	−42	−72	−12	< .001	26

Regions at the conjunction of LFPN task > rest, RFPN task > rest, and DMN rest > task, FWE-corrected $p < .01$ (see Methods section) with a cluster extent of at least 10 voxels. Probabilistic anatomical labels refer to the likelihood that the listed max voxel coordinates are within the given Harvard–Oxford Cortical Structural Atlas region.

($\beta_{LinearAge}$ = 0.56, p = .0016 for Task A subgroup; $\beta_{LinearAge}$ = 0.55, p < .001 for Task B subgroup), such that increasing age was associated with greater task-minus-rest differences in precuneus–LFPN connectivity (Figure 3A). For both tasks, adding a linear age term significantly improved model fit over the intercept-only model ($\chi^2(1)$ = 10.19, p = .0014 for Task A subgroup; $\chi^2(1)$ = 12.65, p < .001 for Task B subgroup). Additional quadratic and cubic age regressors were not significant in models for both tasks (all ps > .05).

We next ran control analyses to examine whether these effects could be attributed to overall task performance or engagement. When learning rate, as a metric of task performance/engagement, was added to the linear age model for Task A (feedback learning task), age remained a significant predictor ($\beta_{LinearAge}$ = 0.51, p = .0070), but learning rate was not a significant predictor ($\beta_{LearningRate}$ = 0.12, p = .39) of task > rest precuneus–LFPN connectivity. When self-reported reward liking, as a metric of task performance/engagement, was added to the linear age

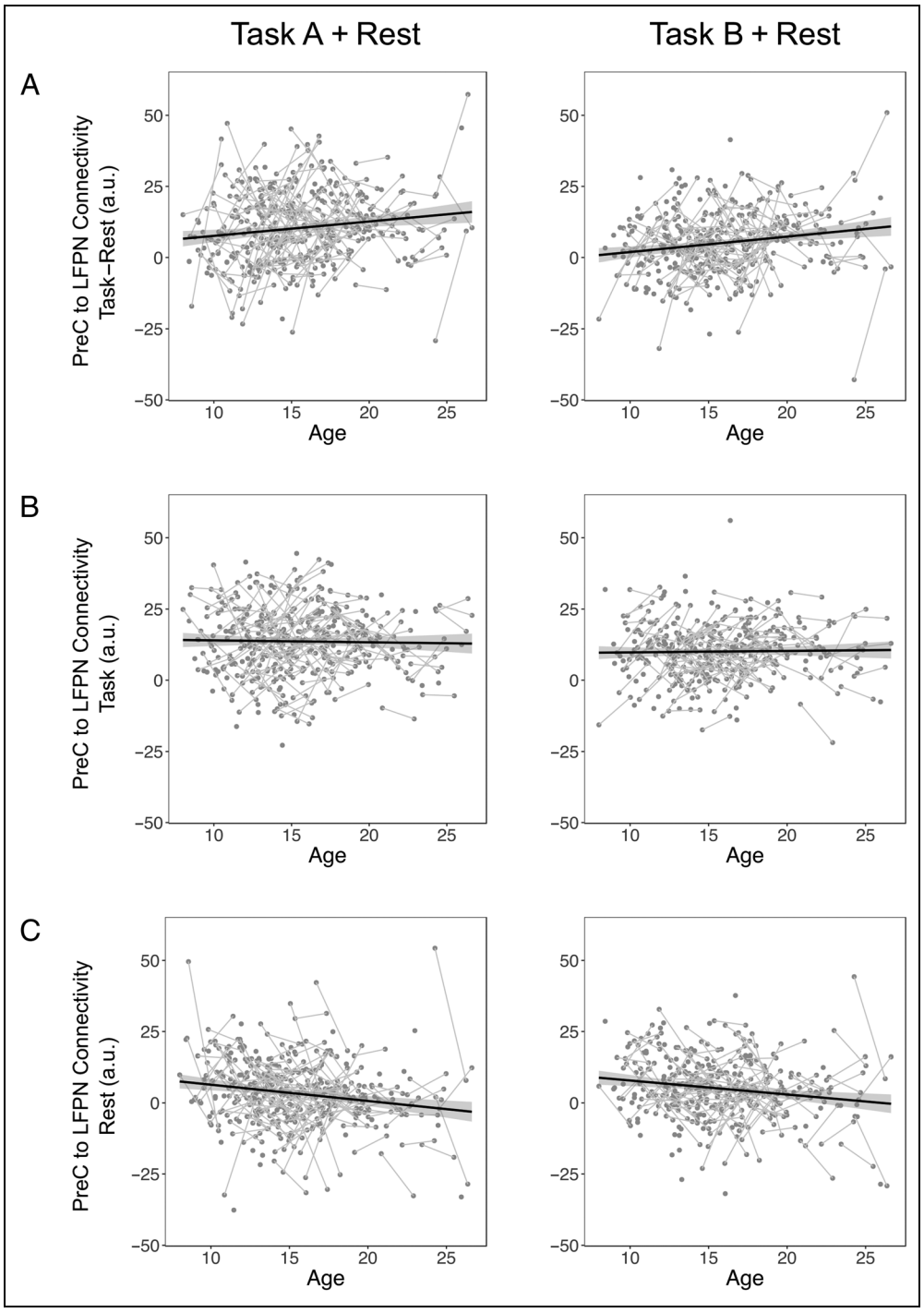

Figure 3. Precuneus–LFPN connectivity changes across development at rest but not task. (A) Across both tasks, task–rest connectivity differences between precuneus and LFPN significantly linearly increased with age. Further probing task connectivity and rest connectivity revealed (B) no significant age-related relationships between precuneus–LFPN connectivity at task but (C) a significant linear age-related decrease in precuneus–LFPN connectivity at rest. Note that the resting-state data in both C panels were drawn from the full set of participants. Each C panel reflects overlapping but different samples that were submitted to separate dual regression analyses. Connected lines link longitudinal data points from the same participant. Shaded areas represent 95% confidence intervals around linear best fit lines.

model for Task B (reward processing task), age remained a significant predictor ($\beta_{LinearAge} = 0.52$, $p = .0037$), but reward liking was not a significant predictor ($\beta_{RewardLiking} = -0.26$, $p = .41$) of task > rest precuneus–LFPN connectivity. Thus, our age-related changes in connectivity cannot be attributed to age-related changes in overall task performance or engagement.

We also ran control analyses to examine whether the relationship between age and precuneus–LFPN task > rest connectivity could be attributed to motion, as measured by a task or rest run's percentage of volumes with *FD* > 0.5 mm. In all cases, adding the percentage of volumes with *FD* > 0.5 mm in the task or rest run to the linear age model resulted in linear age remaining a significant predictor of task > rest precuneus–LFPN connectivity (all *p*s < .014) and percentage of volumes with *FD* > 0.5 mm not being a significant predictor (all *p*s > .33). This is despite the fact that the percentage of volumes with *FD* > 0.5 mm exhibits a significant negative linear relationship with age for both groups across the task and rest data (Task A + Rest subgroup, rest data $\beta = -0.0004$, $p = .0097$, task data $\beta = 0.0009$, $p < .0001$; Task B + Rest subgroup, rest data $\beta = -0.0005$, $p = .0029$, task data $\beta = -0.0012$, $p = .0003$). Thus, whereas motion as measured by the percentage of volumes with *FD* > 0.5 mm does increase linearly with age, linear age remains a significant predictor of task > rest precuneus–LFPN connectivity even after accounting for motion.

We found no significant age-related changes in task-minus-rest precuneus connectivity with DMN and RFPN that replicated across both tasks. There was a significant cubic effect of age on task-minus-rest connectivity between precuneus and DMN in the Task A subgroup ($\beta_{CubicAge} = 0.20$, $p = .035$), but the model with linear, quadratic, and cubic age regressors did not fit significantly better than the intercept only model ($\chi^2(3) = 4.54$, $p = .21$). Furthermore, this cubic effect of age on precuneus–DMN connectivity did not replicate in the Task B subgroup ($\beta_{CubicAge} = -0.0027$, $p = .80$). All other linear, quadratic, and cubic age effects were nonsignificant for task-minus-rest connectivity between precuneus and DMN, and precuneus and RFPN (all *p*s > .05). Thus, although precuneus was significantly more connected to DMN for rest > task and significantly more connected to RFPN for task > rest across the sample and at both time points, no developmental changes were observed in this connectivity.

Connectivity between Precuneus and LFPN Diminishes with Age during Rest but Not Task

To further probe whether the age-related linear increase in task–rest precuneus connectivity with LFPN was due to increased connectivity during task or decreased connectivity during rest, we ran additional mixed models on the connectivity parameters between precuneus and LFPN at task and at rest. For both Task A and Task B, there was no significant linear effect of age upon precuneus–LFPN connectivity during task ($\beta_{LinearAge} = 0.80$, $p = .63$ for Task A; $\beta_{LinearAge} = 0.088$, $p = .55$ for Task B; Figure 3B). Additional models with task engagement and linear age as predictors of precuneus–LFPN connectivity during task found age and task engagement to be nonsignificant predictors in both tasks, and task engagement alone also failed to significantly predict precuneus–LFPN connectivity during task (all predictor *p*s > .05). Thus, precuneus connectivity to the LFPN task-based network neither varied by age nor by task nor by task engagement.

There was, however, a significant linear effect of age during rest ($\beta_{LinearAge} = -0.57$, $p < .001$ for Task A subgroup; $\beta_{LinearAge} = -0.50$, $p = .0020$ for Task B subgroup), such that increasing age was associated with reduced connectivity between precuneus and LFPN at rest (Figure 3C; we reiterate here that the Task A and Task B subgroups represent overlapping but nonidentical samples drawn from the full participant set and submitted to separate dual regression analyses). For both subgroups, adding a linear age term significantly improved model fit over the intercept-only model ($\chi^2(1) = 12.12$, $p < .001$ for Task A subgroup; $\chi^2(1) = 9.86$, $p = .0017$ for Task B subgroup). Additional models with linear age and the percentage of volumes with *FD* > 0.5 mm in the resting-state run found linear age to remain a significant predictor, whereas the percentage of volumes with *FD* > 0.5 mm was not a significant predictor ($\beta_{LinearAge} = -0.58$, $p_{LinearAge} = .0006$, $\beta_{pFD} = -15.71$, $p_{pFD} = .72$ for Task A subgroup; $\beta_{LinearAge} = -.41$, $p_{LinearAge} = .014$, $\beta_{pFD} = 37.03$, $p_{pFD} = .40$ for Task B subgroup). Thus, linear age remains a significant predictor of precuneus–LFPN connectivity at rest, even after accounting for motion.

Additional quadratic age regressors were nonsignificant in the models with linear and quadratic age ($\beta_{QuadraticAge} = 0.014$, $p = .67$ for Task A subgroup; $\beta_{QuadraticAge} = -0.0086$, $p = .78$ for Task B subgroup). In the Task A subgroup, the model with linear, quadratic, and cubic age regressors resulted in a nonsignificant effect of linear age ($\beta_{LinearAge} = -0.030$, $p = .91$) and significant effects of quadratic ($\beta_{QuadraticAge} = 0.085$, $p = .045$) and cubic ($\beta_{CubicAge} = -0.017$, $p = .0089$) age. This cubic age model fit significantly better than the linear age model for the Task A subgroup ($\chi^2(2) = 7.16$, $p = .028$). In the Task B subgroup, however, the cubic age model resulted in nonsignificant regressors for linear, quadratic, and cubic age ($\beta_{LinearAge} = -0.11$, $p = .68$, $\beta_{QuadraticAge} = 0.034$, $p = .40$, and $\beta_{CubicAge} = -0.011$, $p = .087$, respectively), and the cubic age model did not fit significantly better than the linear age model ($\chi^2(2) = 3.07$, $p = .22$). These results suggest that linear age may be a more consistently parsimonious predictor of developmental changes in precuneus–LFPN connectivity at rest.

DISCUSSION

In this study, we investigated the state-dependent functional connectivity of the precuneus across development

in a large cross-sectional and longitudinal sample of participants between the ages of 8 and 26 years. Previous work has shown that the precuneus serves as a unique hub distinguishing between task and rest states in the adult brain (Utevsky et al., 2014), yet little has been known about the role of precuneus in the developing brain. Using dual regression analyses to track network-based functional connectivity across the sample, we show that the precuneus exhibits both greater functional connectivity with two task-based networks (RFPN and LFPN) during task compared with rest, as well as greater functional connectivity with the rest-based DMN during rest compared with task. This result replicated across two different tasks and at two longitudinal time points. Thus, the role of precuneus in mediating between task and rest states is evident throughout development from childhood through early adulthood.

We next examined whether the mediating function of the precuneus strengthens or matures over development by searching for age-related changes in state-dependent functional connectivity between precuneus and LFPN, RFPN, and DMN. Across two distinct tasks, we found a significant linear age-related increase in state-dependent functional connectivity between precuneus and LFPN, such that task > rest connectivity between precuneus and LFPN significantly linearly increased with age from childhood to adulthood. We determined that the relationship between age and task > rest precuneus–LFPN connectivity was driven by an age-related decrease in precuneus–LFPN connectivity during rest. Such age-related increasing segregation between LFPN and a region of DMN during rest is consistent with prior work showing age-related increases in network segregation in both structural (Baum et al., 2017) and resting-state data (Sherman et al., 2014; Uddin et al., 2011; Fair et al., 2007, 2008). We note that our developmental findings are strengthened by BrainTime's accelerated longitudinal design, in which both cross-sectional and longitudinal effects can be captured.

In contrast to the observed developmental connectivity changes during rest, task-related connectivity between precuneus and LFPN was continuously high across ages and showed no developmental changes. This suggests that age-related increases in network segregation shown during rest (Sherman et al., 2014; Uddin et al., 2011; Fair et al., 2007, 2008) may not occur during task and/or do not apply to precuneus–LFPN connectivity. Finally, we found that precuneus's state-dependent connectivity with DMN (rest > task) and RFPN (task > rest) remained developmentally stable, with no significant effect of linear, quadratic, and/or cubic age.

Notably, we did not find task performance or engagement to significantly predict task > rest precuneus–LFPN connectivity after accounting for the effect of age. Furthermore, we found no significant relationship between individuals' task performance or engagement and their precuneus–LFPN connectivity during task. This is surprising, given that prior work has shown that different tasks differentially affect segregation and integration between neural networks (Khambhati, Medaglia, Karuza, Thompson-Schill, & Bassett, 2018; Cohen & D'Esposito, 2016), that task performance affects the FPN's overall activation and functional connectivity throughout the brain (Dwyer et al., 2014; Cole et al., 2013; Satterthwaite, Wolf, et al., 2013), and that DMN–RFPN connectivity facilitates response time in a memory task (Fornito et al., 2012). Thus, our findings highlight the unique role of the precuneus, which tracks whether the brain is engaged in a task state generally, with no observed differences between the two tasks in the BrainTime data set. Future work could investigate whether precuneus–LFPN connectivity is moderated by task engagement for more variably engaging/demanding tasks (e.g., n-back tasks with varying n as in Cohen & D'Esposito, 2016; Satterthwaite, Wolf, et al., 2013). Application of network-based psychophysiological interaction approaches (Utevsky, Smith, Young, & Huettel, 2017) can also be used to determine whether the time course of precuneus–LFPN connectivity is modulated by moment-to-moment changes in task demands (e.g., precuneus–LFPN connectivity for high demand > low demand blocks within the same run).

We note that this study replicates the previous findings of Utevsky and colleagues' (2014) study of adult neural data and extends them in three significant ways. First, we extend the findings to a large cross-sectional and longitudinal developmental sample, which allowed us to show that the role of precuneus as a functional core of the DMN is in place in childhood. The developmental trajectory of task > rest precuneus–LFPN connectivity suggests, however, that younger populations than those in our sample (e.g., children younger than 8 years) may exhibit no differences in precuneus–LFPN connectivity for task versus rest states. Thus, future work could examine precuneus connectivity in even younger participants to determine if this is, in fact, the case. Second, our work further extends the precuneus connectivity finding to two tasks different from those used in the adult study (Utevsky et al., 2014). This strengthens the hypothesis that precuneus mediates between rest and task generally, regardless of the specific task. Third, our study complements prior work: Although the previous adult study collected the resting-state scan last, after the completion of the three tasks (Utevsky et al., 2014), our study collected the resting-state scan first, before the task runs. This avoids the concern that recent exposure to a task may alter subsequent resting-state connectivity (Tung et al., 2013; Stevens, Buckner, & Schacter, 2010; Waites, Stanislavsky, Abbott, & Jackson, 2005). Thus, the two studies together suggest that the precuneus's unique role in mediating between task and rest states holds, regardless of task versus rest order.

Prior studies investigating developmental changes in whole-brain connectivity patterns have often used graph-theoretical approaches that examine connectivity

strength between distributed nodes (Fair et al., 2007, 2008; see Stevens, 2016; Ernst, Torrisi, Balderston, Grillon, & Hale, 2015; Power, Fair, Schlaggar, & Petersen, 2010, for reviews). Such developmental work, however, generally investigates connectivity during rest rather than during task (but see Joseph et al., 2012) and do not directly compare across task and rest states, as in this study. Given that graph theory analyses have also implicated precuneus as a key functional hub during rest (Tomasi & Volkow, 2010) and have been applied to understand changes in task-versus rest-based functional connectivity in adult brains (Bolt, Nomi, Rubinov, & Uddin, 2017; Cole, Bassett, Power, Braver, & Petersen, 2014), combining dual regression and task-versus-rest analyses with graph theory approaches could be complementary and yield further insight as to how neural hubs affect processing state.

This study's connectivity analyses were applied to task and rest scans ranging from approximately 5 to 8 min. Although previous work has shown that this duration is suitable for stable estimates of connectivity networks (Van Dijk et al., 2010; Fox et al., 2005), the reliability of connectivity estimates is also known to increase with scan time, plateauing around 12 min (Birn et al., 2013). This study also used 0.5 mm as the *FD* threshold (Power et al., 2012) for spike regression, whereas more recent work has used even more stringent *FD* thresholds of 0.25 mm (Parkes, Fulcher, Yücel, & Fornito, 2018; Satterthwaite, Elliott, et al., 2013) or 0.2 mm (Ciric et al., 2017). Future work could use longer task- and rest-based fMRI scans with more stringent motion thresholds to determine if our findings replicate under longer durations and stricter motion correction.

Additional future studies could also use structural neuroimaging techniques, such as diffusion tensor imaging, to determine whether developmental changes in precuneus–LFPN functional connectivity are reflected in structural changes in the developing brain. Converging evidence from nonhuman primate anatomical tracing studies (Leichnetz, 2001) and resting-state functional connectivity work in humans and nonhuman primates (Margulies et al., 2009) suggest that there are cortical projections between precuneus and regions of the LFPN, including lateral pFC and lateral parietal cortex (Cavanna & Trimble, 2006). Future work should examine whether and how such structural connections between precuneus and LFPN underlie state-dependent differences in functional connectivity and how they may change across development.

It is important to understand developmental changes in task- and rest-state connectivity, as altered connectivity has been reported for numerous psychological disorders (see Cohen, 2018; Greicius, 2008, for reviews). For example, a maturational lag in DMN-to-FPN connectivity has been associated with attention-deficit/hyperactivity disorder (Sripada, Kessler, & Angstadt, 2014), and abnormal resting-state functional connectivity between DMN and FPN has been found in patients with obsessive compulsive disorder (Stern, Fitzgerald, Welsh, Abelson, & Taylor, 2012) and with impaired consciousness (Long et al., 2016). Future work could investigate whether precuneus's task- and rest-based connectivity is altered in atypical development and whether any such deviations from typical connectivity development correspond to behavioral or psychological impairments.

In this study, we demonstrate that precuneus plays a key role in mediating between task and rest states via connectivity with DMN and FPNs across typical development. These results underscore the unique nature of an enigmatic brain region that has been implicated in processes as varied as memory, self-processing, decision-making, and even consciousness (Cavanna & Trimble, 2006), while also pointing to future targets for understanding changes in neural connectivity in typical and atypical development.

Acknowledgments

This work was supported by an innovative ideas grant of the European Research Council (ERC-2010-StG-263234) to E. A. C. and a Graduate Research Opportunities Worldwide Fellowship from the National Science Foundation and the Netherlands Organisation for Scientific Research to R. L.

Reprint requests should be sent to Rosa Li, Box 90999, Durham, NC 27708, or via e-mail: rosaliphd@gmail.com or Anna C. K. van Duijvenvoorde, Wassenaarseweg 52, 2333 AK Leiden, Room 3B34, or via e-mail: a.c.k.van.duijvenvoorde@fsw.leidenuniv.nl.

REFERENCES

Baum, G. L., Ciric, R., Roalf, D. R., Betzel, R. F., Moore, T. M., Shinohara, R. T., et al. (2017). Modular segregation of structural brain networks supports the development of executive function in youth. *Current Biology*, *27*, 1561.e8–1572.e8.

Beckmann, C. F., & Smith, S. M. (2004). Probabilistic independent component analysis for functional magnetic resonance imaging. *IEEE Transactions on Medical Imaging*, *23*, 137–152.

Birn, R. M., Molloy, E. K., Patriat, R., Parker, T., Meier, T. B., Kirk, G. R., et al. (2013). The effect of scan length on the reliability of resting-state fMRI connectivity estimates. *Neuroimage*, *83*, 550–558.

Bolt, T., Nomi, J. S., Rubinov, M., & Uddin, L. Q. (2017). Correspondence between evoked and intrinsic functional brain network configurations. *Human Brain Mapping*, *38*, 1992–2007.

Braams, B. R., & Crone, E. A. (2017a). Longitudinal changes in social brain development: Processing outcomes for friend and self. *Child Development*, *88*, 1952–1965.

Braams, B. R., & Crone, E. A. (2017b). Peers and parents: A comparison between neural activation when winning for friends and mothers in adolescence. *Social Cognitive and Affective Neuroscience*, *12*, 417–426.

Braams, B. R., Güroğlu, B., de Water, E., Meuwese, R., Koolschijn, P. C., Peper, J. S., et al. (2014). Reward-related neural responses are dependent on the beneficiary. *Social Cognitive and Affective Neuroscience*, *9*, 1030–1037.

Braams, B. R., Peper, J. S., Van Der Heide, D., Peters, S., & Crone, E. A. (2016). Nucleus accumbens response to rewards and testosterone levels are related to alcohol use in adolescents and young adults. *Developmental Cognitive Neuroscience*, *17*, 83–93.

Braams, B. R., Peters, S., Peper, J. S., Güroğlu, B., & Crone, E. A. (2014). Gambling for self, friends, and antagonists: Differential contributions of affective and social brain regions on adolescent reward processing. *Neuroimage*, *100*, 281–289.

Braams, B. R., van Duijvenvoorde, A. C., Peper, J. S., & Crone, E. A. (2015). Longitudinal changes in adolescent risk-taking: A comprehensive study of neural responses to rewards, pubertal development, and risk-taking behavior. *Journal of Neuroscience*, *35*, 7226–7238.

Cavanna, A. E., & Trimble, M. R. (2006). The precuneus: A review of its functional anatomy and behavioural correlates. *Brain*, *129*, 564–583.

Ciric, R., Wolf, D. H., Power, J. D., Roalf, D. R., Baum, G. L., Ruparel, K., et al. (2017). Benchmarking of participant-level confound regression strategies for the control of motion artifact in studies of functional connectivity. *Neuroimage*, *154*, 174–187.

Cohen, J. R. (2018). The behavioral and cognitive relevance of time-varying, dynamic changes in functional connectivity. *Neuroimage*, *180*, 515–525.

Cohen, J. R., & D'Esposito, M. (2016). The segregation and integration of distinct brain networks and their relationship to cognition. *Journal of Neuroscience*, *36*, 12083–12094.

Cole, M. W., Bassett, D. S., Power, J. D., Braver, T. S., & Petersen, S. E. (2014). Intrinsic and task-evoked network architectures of the human brain. *Neuron*, *83*, 238–251.

Cole, M. W., Reynolds, J. R., Power, J. D., Repovs, G., Anticevic, A., & Braver, T. S. (2013). Multi-task connectivity reveals flexible hubs for adaptive task control. *Nature Neuroscience*, *16*, 1348–1355.

Corbetta, M., & Shulman, G. L. (2002). Control of goal-directed and stimulus-driven attention in the brain. *Nature Reviews Neuroscience*, *3*, 201–215.

Desikan, R. S., Ségonne, F., Fischl, B., Quinn, B. T., Dickerson, B. C., Blacker, D., et al. (2006). An automated labeling system for subdividing the human cerebral cortex on MRI scans into gyral based regions of interest. *Neuroimage*, *31*, 968–980.

Dwyer, D. B., Harrison, B. J., Yücel, M., Whittle, S., Zalesky, A., Pantelis, C., et al. (2014). Large-scale brain network dynamics supporting adolescent cognitive control. *Journal of Neuroscience*, *34*, 14096–14107.

Ernst, M., Torrisi, S., Balderston, N., Grillon, C., & Hale, E. A. (2015). fMRI functional connectivity applied to adolescent neurodevelopment. *Annual Review of Clinical Psychology*, *11*, 361–377.

Fair, D. A., Cohen, A. L., Dosenbach, N. U., Church, J. A., Miezin, F. M., Barch, D. M., et al. (2008). The maturing architecture of the brain's default network. *Proceedings of the National Academy of Sciences, U.S.A.*, *105*, 4028–4032.

Fair, D. A., Cohen, A. L., Power, J. D., Dosenbach, N. U., Church, J. A., Miezin, F. M., et al. (2009). Functional brain networks develop from a "local to distributed" organization. *PLoS Computational Biology*, *5*, e1000381.

Fair, D. A., Dosenbach, N. U., Church, J. A., Cohen, A. L., Brahmbhatt, S., Miezin, F. M., et al. (2007). Development of distinct control networks through segregation and integration. *Proceedings of the National Academy of Sciences, U.S.A.*, *104*, 13507–13512.

Filippi, M., Valsasina, P., Misci, P., Falini, A., Comi, G., & Rocca, M. A. (2013). The organization of intrinsic brain activity differs between genders: A resting-state fMRI study in a large cohort of young healthy subjects. *Human Brain Mapping*, *34*, 1330–1343.

Filippini, N., MacIntosh, B. J., Hough, M. G., Goodwin, G. M., Frisoni, G. B., Smith, S. M., et al. (2009). Distinct patterns of brain activity in young carriers of the APOE- 4 allele. *Proceedings of the National Academy of Sciences, U.S.A.*, *106*, 7209–7214.

Fletcher, P. C., Frith, C. D., Baker, S. C., Shallice, T., Frackowiak, R. S., & Dolan, R. J. (1995). The mind's eye—Precuneus activation in memory-related imagery. *Neuroimage*, *2*, 195–200.

Fornito, A., Harrison, B. J., Zalesky, A., & Simons, J. S. (2012). Competitive and cooperative dynamics of large-scale brain functional networks supporting recollection. *Proceedings of the National Academy of Sciences, U.S.A.*, *109*, 12788–12793.

Fox, M. D., Snyder, A. Z., Vincent, J. L., Corbetta, M., Van Essen, D. C., & Raichle, M. E. (2005). The human brain is intrinsically organized into dynamic, anticorrelated functional networks. *Proceedings of the National Academy of Sciences, U.S.A.*, *102*, 9673–9678.

Friedman, L., Glover, G. H., & The FBIRN Consortium. (2006). Reducing interscanner variability of activation in a multicenter fMRI study: Controlling for signal-to-fluctuation-noise-ratio (SFNR) differences. *Neuroimage*, *33*, 471–481.

Greicius, M. (2008). Resting-state functional connectivity in neuropsychiatric disorders. *Current Opinion in Neurology*, *21*, 424–430.

Hayden, B. Y., Nair, A. C., McCoy, A. N., & Platt, M. L. (2008). Posterior cingulate cortex mediates outcome-contingent allocation of behavior. *Neuron*, *60*, 19–25.

Honey, C. J., Sporns, O., Cammoun, L., Gigandet, X., Thiran, J. P., Meuli, R., et al. (2009). Predicting human resting-state functional connectivity from structural connectivity. *Proceedings of the National Academy of Sciences, U.S.A.*, *106*, 2035–2040.

Jenkinson, M., & Smith, S. M. (2001). A global optimisation method for robust affine registration of brain images. *Medical Image Analysis*, *5*, 143–156.

Joseph, J. E., Swearingen, J. E., Clark, J. D., Benca, C. E., Collins, H. R., Corbly, C. R., et al. (2012). The changing landscape of functional brain networks for face processing in typical development. *Neuroimage*, *63*, 1223–1236.

Khambhati, A. N., Medaglia, J. D., Karuza, E. A., Thompson-Schill, S. L., & Bassett, D. S. (2018). Subgraphs of functional brain networks identify dynamical constraints of cognitive control. *PLOS Computational Biology*, *14*, e1006234.

Leech, R., Braga, R., & Sharp, D. J. (2012). Echoes of the brain within the posterior cingulate cortex. *Journal of Neuroscience*, *32*, 215–222.

Leech, R., Kamourieh, S., Beckmann, C. F., & Sharp, D. J. (2011). Fractionating the default mode network: Distinct contributions of the ventral and dorsal posterior cingulate cortex to cognitive control. *Journal of Neuroscience*, *31*, 3217–3224.

Leichnetz, G. R. (2001). Connections of the medial posterior parietal cortex (area 7m) in the monkey. *Anatomical Record*, *263*, 215–236.

Long, J., Xie, Q., Ma, Q., Urbin, M. A., Liu, L., Weng, L., et al. (2016). Distinct interactions between fronto-parietal and default mode networks in impaired consciousness. *Scientific Reports*, *6*, 38866.

Lundstrom, B. N., Ingvar, M., & Petersson, K. M. (2005). The role of precuneus and left inferior frontal cortex during source memory episodic retrieval. *Neuroimage*, *27*, 824–834.

Maddock, R. J., Garrett, A. S., & Buonocore, M. H. (2001). Remembering familiar people: The posterior cingulate cortex and autobiographical memory retrieval. *Neuroscience*, *104*, 667–676.

Maddock, R. J., Garrett, A. S., & Buonocore, M. H. (2003). Posterior cingulate cortex activation by emotional words:

fMRI evidence from a valence decision task. *Human Brain Mapping*, *18*, 30–41.
Madhyastha, T., Peverill, M., Koh, N., McCabe, C., Flournoy, J., Mills, K., et al. (2018). Current methods and limitations for longitudinal fMRI analysis across development. *Developmental Cognitive Neuroscience*, *33*, 118–128.
Margulies, D. S., Vincent, J. L., Kelly, C., Lohmann, G., Uddin, L. Q., Biswal, B. B., et al. (2009). Precuneus shares intrinsic functional architecture in humans and monkeys. *Proceedings of the National Academy of Sciences, U.S.A.*, *106*, 20069–20074.
Nichols, T., Brett, M., Andersson, J., Wager, T., & Poline, J.-B. (2005). Valid conjunction inference with the minimum statistic. *Neuroimage*, *25*, 653–660.
Nickerson, L. D., Smith, S. M., Öngür, D., & Beckmann, C. F. (2017). Using dual regression to investigate network shape and amplitude in functional connectivity analyses. *Frontiers in Neuroscience*, *11*, 115.
Parkes, L., Fulcher, B., Yücel, M., & Fornito, A. (2018). An evaluation of the efficacy, reliability, and sensitivity of motion correction strategies for resting-state functional MRI. *Neuroimage*, *171*, 415–436.
Peters, S., Braams, B. R., Raijmakers, M. E., Koolschijn, P. C., & Crone, E. A. (2014). The neural coding of feedback learning across child and adolescent development. *Journal of Cognitive Neuroscience*, *26*, 1705–1720.
Peters, S., & Crone, E. A. (2017). Increased striatal activity in adolescence benefits learning. *Nature Communications*, *8*, 1983.
Peters, S., Jolles, D. J., van Duijvenvoorde, A. C., Crone, E. A., & Peper, J. S. (2015). The link between testosterone and amygdala-orbitofrontal cortex connectivity in adolescent alcohol use. *Psychoneuroendocrinology*, *53*, 117–126.
Peters, S., Koolschijn, P. C., Crone, E. A., van Duijvenvoorde, A. C., & Raijmakers, M. E. (2014). Strategies influence neural activity for feedback learning across child and adolescent development. *Neuropsychologia*, *62*, 365–374.
Peters, S., Peper, J. S., van Duijvenvoorde, A. C. K., Braams, B. R., & Crone, E. A. (2017). Amygdala–orbitofrontal connectivity predicts alcohol use two years later: A longitudinal neuroimaging study on alcohol use in adolescence. *Developmental Science*, *20*, e12448.
Peters, S., Van der Meulen, M., Zanolie, K., & Crone, E. A. (2017). Predicting reading and mathematics from neural activity for feedback learning. *Developmental Psychology*, *53*, 149–159.
Peters, S., Van Duijvenvoorde, A. C., Koolschijn, P. C., & Crone, E. A. (2016). Longitudinal development of frontoparietal activity during feedback learning: Contributions of age, performance, working memory and cortical thickness. *Developmental Cognitive Neuroscience*, *19*, 211–222.
Pinheiro, J., Bates, D., DebRoy, S., Sarkar, D., & R Core Team. (2019). *nlme: Linear and nonlinear mixed effects models*. R package version 3.1-141, https://CRAN.R-project.org/package=nlme.
Power, J. D., Barnes, K. A., Snyder, A. Z., Schlaggar, B. L., & Petersen, S. E. (2012). Spurious but systematic correlations in functional connectivity MRI networks arise from subject motion. *Neuroimage*, *59*, 2142–2154.
Power, J. D., Fair, D. A., Schlaggar, B. L., & Petersen, S. E. (2010). The development of human functional brain networks. *Neuron*, *67*, 735–748.
Raichle, M. E., MacLeod, A. M., Snyder, A. Z., Powers, W. J., Gusnard, D. A., & Shulman, G. L. (2001). A default mode of brain function. *Proceedings of the National Academy of Sciences, U.S.A.*, *98*, 676–682.
Satterthwaite, T. D., Elliott, M. A., Gerraty, R. T., Ruparel, K., Loughead, J., Calkins, M. E., et al. (2013). An improved framework for confound regression and filtering for control of motion artifact in the preprocessing of resting-state functional connectivity data. *Neuroimage*, *64*, 240–256.
Satterthwaite, T. D., Wolf, D. H., Erus, G., Ruparel, K., Elliott, M. A., Gennatas, E. D., et al. (2013). Functional maturation of the executive system during adolescence. *Journal of Neuroscience*, *33*, 16249–16261.
Satterthwaite, T. D., Wolf, D. H., Loughead, J., Ruparel, K., Elliott, M. A., Hakonarson, H., et al. (2012). Impact of in-scanner head motion on multiple measures of functional connectivity: Relevance for studies of neurodevelopment in youth. *Neuroimage*, *60*, 623–632.
Schreuders, E., Braams, B. R., Blankenstein, N. E., Peper, J. S., Güroğlu, B., & Crone, E. A. (2018). Contributions of reward sensitivity to ventral striatum activity across adolescence and early adulthood. *Child Development*, *89*, 797–810.
Sherman, L. E., Rudie, J. D., Pfeifer, J. H., Masten, C. L., McNealy, K., & Dapretto, M. (2014). Development of the default mode and central executive networks across early adolescence: A longitudinal study. *Developmental Cognitive Neuroscience*, *10*, 148–159.
Shulman, G. L., Fiez, J. A., Corbetta, M., Buckner, R. L., Miezin, F. M., Raichle, M. E., et al. (1997). Common blood flow changes across visual tasks: II. Decreases in cerebral cortex. *Journal of Cognitive Neuroscience*, *9*, 648–663.
Smith, S. M. (2002). Fast robust automated brain extraction. *Human Brain Mapping*, *17*, 143–155.
Smith, S. M., Fox, P. T., Miller, K. L., Glahn, D. C., Fox, P. M., Mackay, C. E., et al. (2009). Correspondence of the brain's functional architecture during activation and rest. *Proceedings of the National Academy of Sciences, U.S.A.*, *106*, 13040–13045.
Smith, S. M., Jenkinson, M., Woolrich, M. W., Beckmann, C. F., Behrens, T. E., Johansen-Berg, H., et al. (2004). Advances in functional and structural MR image analysis and implementation as FSL. *Neuroimage*, *23*, S208–S219.
Smith, S. M., & Nichols, T. E. (2009). Threshold-free cluster enhancement: Addressing problems of smoothing, threshold dependence and localisation in cluster inference. *Neuroimage*, *44*, 83–98.
Smith, D. V., Utevsky, A. V., Bland, A. R., Clement, N., Clithero, J. A., Harsch, A. E., et al. (2014). Characterizing individual differences in functional connectivity using dual-regression and seed-based approaches. *Neuroimage*, *95*, 1–12.
Sripada, C. S., Kessler, D., & Angstadt, M. (2014). Lag in maturation of the brain's intrinsic functional architecture in attention-deficit/hyperactivity disorder. *Proceedings of the National Academy of Sciences, U.S.A.*, *111*, 14259–14264.
Stern, E. R., Fitzgerald, K. D., Welsh, R. C., Abelson, J. L., & Taylor, S. F. (2012). Resting-state functional connectivity between fronto-parietal and default mode networks in obsessive-compulsive disorder. *PLOS ONE*, *7*, e36356.
Stevens, M. C. (2016). The contributions of resting state and task-based functional connectivity studies to our understanding of adolescent brain network maturation. *Neuroscience and Biobehavioral Reviews*, *70*, 13–32.
Stevens, W. D., Buckner, R. L., & Schacter, D. L. (2010). Correlated low-frequency BOLD fluctuations in the resting human brain are modulated by recent experience in category-preferential visual regions. *Cerebral Cortex*, *20*, 1997–2006.
Tomasi, D., & Volkow, N. D. (2010). Functional connectivity density mapping. *Proceedings of the National Academy of Sciences, U.S.A.*, *107*, 9885–9890.
Tung, K. C., Uh, J., Mao, D., Xu, F., Xiao, G., & Lu, H. (2013). Alterations in resting functional connectivity due to recent motor task. *Neuroimage*, *78*, 316–324.
Uddin, L. Q., Supekar, K. S., Ryali, S., & Menon, V. (2011). Dynamic reconfiguration of structural and functional connectivity across core neurocognitive brain networks with development. *Journal of Neuroscience*, *31*, 18578–18589.

Utevsky, A. V., Smith, D. V., & Huettel, S. A. (2014). Precuneus is a functional core of the default-mode network. *Journal of Neuroscience*, *34*, 932–940.
Utevsky, A. V., Smith, D. V., Young, J. S., & Huettel, S. A. (2017). Large-scale network coupling with the fusiform cortex facilitates future social motivation. *Eneuro*, *4*, ENEURO.0084-17.2017.
van den Heuvel, M. P., & Hulshoff Pol, H. E. (2010). Exploring the brain network: A review on resting-state fMRI functional connectivity. *European Neuropsychopharmacology*, *20*, 519–534.
van Dijk, K. R., Hedden, T., Venkataraman, A., Evans, K. C., Lazar, S. W., & Buckner, R. L. (2010). Intrinsic functional connectivity as a tool for human connectomics: Theory, properties, and optimization. *Journal of Neurophysiology*, *103*, 297–321.
van Duijvenvoorde, A. C. K., Achterberg, M., Braams, B. R., Peters, S., & Crone, E. A. (2015). Testing a dual-systems model of adolescent brain development using resting-state connectivity analyses. *Neuroimage*, *124*, 409–420.
van Duijvenvoorde, A. C. K., Westhoff, B., de Vos, F., Wierenga, L. M., & Crone, E. A. (2019). A three-wave longitudinal study of subcortical-cortical resting-state connectivity in adolescence: Testing age- and puberty-related changes. *Human Brain Mapping*, *40*, 3769–3783.
Vincent, J. L., Kahn, I., Snyder, A. Z., Raichle, M. E., & Buckner, R. L. (2008). Evidence for a frontoparietal control system revealed by intrinsic functional connectivity. *Journal of Neurophysiology*, *100*, 3328–3342.
Waites, A. B., Stanislavsky, A., Abbott, D. F., & Jackson, G. D. (2005). Effect of prior cognitive state on resting state networks measured with functional connectivity. *Human Brain Mapping*, *24*, 59–68.
Winkler, A. M., Ridgway, G. R., Webster, M. A., Smith, S. M., & Nichols, T. E. (2014). Permutation inference for the general linear model. *Neuroimage*, *92*, 381–397.
Woolrich, M. W., Jbabdi, S., Patenaude, B., Chappell, M., Makni, S., Behrens, T., et al. (2009). Bayesian analysis of neuroimaging data in FSL. *Neuroimage*, *45*, S173–S186.